Structural transition in $(C_{60})_n$ clusters

W. Branz, N. Malinowski,* A. Enders, and T. P. Martin
Max-Planck-Institut für Festkörperforschung, Heisenbergstrasse 1, 70569 Stuttgart, Germany
(Received 21 March 2002; published 17 September 2002)

The structure of $(C_{60})_n$ clusters ($n=1-150$) was investigated by heating them to definite temperatures in a helium bath (heating cell) with subsequent characterization in a time-of-flight mass spectrometer. The intensity anomalies in the resulting mass spectra reflect particularly stable configurations that resisted evaporation. However, the set of enhanced peaks (magic numbers) turned out to be temperature dependent. Clusters heated to a moderate temperature of 490 K yielded mass spectra indicating the presence of icosahedral structures that can be characterized by a set of unusually strong peaks, namely $n=13, 19, 23, 26, 35, 39, 43, 46, 49, 55, 55+3m$, 116, 125, 131, 137, and 147 ($m=1-14$). Based on constant-temperature molecular dynamics simulations it could be concluded that these icosahedra represent metastable structures that had not yet attained thermal equilibrium on the experimental time scale ($t_s=0.5$ ms). Only when the $(C_{60})_n$ clusters were heated to appreciably higher temperatures they could reach thermodynamical equilibrium, manifested by a thermally induced structural transition into close-packed structures, decahedral structures and structures based on the 98-Leary tetrahedron. Thus, mass spectra of clusters heated to 600 K demonstrate the new set of magic numbers, $n=38, 48, 58, 61, 64, 68, 71, 75, 77, 84, 89, 91, 96$, and 98. Additionally, the experimental arrangement used allows both charged and neutral $(C_{60})_n$ clusters to be studied. Thereby, it was possible to show that the structure of large $(C_{60})_n$ clusters is insensitive to their charge state ($-/n/+$), disproving a hypothesis that has been discussed in the literature for several years. The heating cell was also used to study the thermally induced dissociation in the fullerene dimers $(C_{60})_2$, $(C_{70})_2$, and $(C_{60})_2^+$. The dissociation energies were determined to be 0.275 eV, 0.313 eV, and 0.37 eV, respectively (± 0.08 eV).

DOI: 10.1103/PhysRevB.66.094107 PACS number(s): 61.46.+w, 36.40.−c, 61.48.+c

I. INTRODUCTION

After the discovery of the large scale C_{60} synthesis,[1] the properties of fullerene solids have been intensively investigated. As the intermolecular C_{60} potential is very short ranged compared to the large fullerene diameter, C_{60} molecules might be regarded as ''nanoscopic hard spheres.'' Therefore it is not very surprising that in a C_{60} crystal the molecules are placed on the fcc close-packed sites expected for hard spheres.[2] However, some bulk properties are also very sensitive to the exact shape of the unusually narrow potential well. So it is, for example, not yet clear if C_{60} has a slightly stable liquid phase[3–6] or not.[7,8]

Several years ago the observation of clusters of C_{60} molecules stimulated considerable interest in their structure.[9] The intensity anomalies in the photofragmentation mass spectra of positively charged $(C_{60})_n$ clusters clearly indicated the presence of structures based on Mackay icosahedra.[10] The especially high stability of the $(C_{60})_{13}$ icosahedron was also demonstrated by experiments of Hansen *et al.*[11,12] In all these experiments the heating of the clusters was accomplished by a short excimer laser pulse ($\Delta t \approx 15$ ns). However, the experimental results contradicted subsequent theoretical studies on the structure of $(C_{60})_n$ clusters. Although there is still controversy about the most suitable intermolecular C_{60} potential,[13–23] to date all global optimization calculations predict close-packed or decahedral structures for $(C_{60})_n$ clusters above a certain crossover cluster size in the range between $n=13$ and 16.[22–28] For example, when the spherically averaged Girifalco (GF) potential is used, icosahedral structures represent only the global energy minima up to $n=13$.[22,24] Even with a full 60-site atom-atom potential, the crossover shifts only slightly to larger sizes ($n=16$).[23,25,26] Recently, Pacheco and Prates-Ramalho (PPR) published a new intermolecular C_{60} potential that was obtained from *ab initio* calculations of solid C_{60}.[14] When compared with the Girifalco potential, the PPR potential indeed gives a better description of some bulk properties, such as, for example, the volume-pressure dependence.[14] However, structure calculations for PPR clusters also failed in explaining the appearance of icosahedral structures in $(C_{60})_n$ clusters, even if the additional three-body term of the PPR potential was included.[27,28] The sizes where close-packed and decahedral structures appear are $n=15$ for the three-body and $n=16$ in the case of the two-body PPR potential.[28] The general reason for this rapid disappearance of icosahedral global minima at small cluster sizes is the short-ranged intermolecular potential. With the decreasing range of the potential, structures with high internal strain, such as icosahedra or disordered liquidlike configurations, are energetically less favorable because they involve nearest-neighbor distances that deviate from the equilibrium pair separation.[29,30]

One possible explanation for the discrepancy between the experimental and theoretical findings that has been discussed for several years in the literature is the suggestion that all calculations were performed for neutral clusters, whereas the mass spectra of Martin et al. allow conclusions only for positively charged clusters.[22,25,26] Indeed, due to the large polarizability of the C_{60} molecule,[31] it seems not unlikely that the introduction of a long-range Coulomb term could fundamentally influence the structure of fullerene clusters. In order to test this hypothesis we have performed a more detailed ex-

perimental investigation of both charged and neutral $(C_{60})_n$ clusters.[32] In the present work we show experimental data clearly indicating that the structure of $(C_{60})_n$ clusters is indeed independent from their charge state.

Although the cluster charge has little influence on their structure, another parameter does—the cluster *temperature*. In contrast to the former laser heating experiments, in the new experiments the clusters were heated by a helium bath as described in detail below. When annealing the clusters at comparatively low temperatures, e.g., at $T_h = 490$ K for a time span of ca. 0.5 ms, in principle, the same icosahedral magic numbers as in the spectra yielded by laser heating were obtained.[32] At higher temperatures (e.g., $T_h = 600$ K) the set of magic numbers completely changes and has been interpreted as a thermally induced structural transition to close-packed and decahedral structures and also structures based on the recently discovered 98-Leary tetrahedron.[33] These structural assignments were confirmed by structural calculations on $(C_{60})_n$ clusters modeled by the PPR potential.[28]

The experimental findings pose a challenge for a theoretical description. A temperature-dependent set of magic numbers cannot be explained only by global optimization calculations, but thermodynamics and kinetics have to play the key role for the understanding of the observed effects. Furthermore, for theoretically examined systems, icosahedral structures were preferred at *high* temperatures because of their larger vibrational entropy.[34–39] These results give a first hint that the icosahedral structures occurring for $(C_{60})_n$ clusters at low temperatures are most probably due to thermodynamical *nonequilibrium* conditions. Such a metastable icosahedral phase has been observed in growth simulations of silver clusters[40] and the same method has very recently given evidence for kinetic trapping effects in icosahedral structures for $(C_{60})_n$ clusters.[41] In this paper we will discuss the thermally induced structural transition in $(C_{60})_n$ clusters in greater detail by the presentation of new experimental and theoretical results.

II. EXPERIMENTAL METHOD

The fullerene clusters were studied by the technique of time-of-flight (TOF) mass spectrometry. In our new Reflectron TOF (Ref. 42) we applied high acceleration ($U_{acc} = 18$ kV) and post acceleration ($U_{post} = 30$ kV) voltages in order to avoid detection problems for large, singly charged clusters ($n > 100$). For such large clusters only a weak signal could be achieved in our old machine.[9] As cluster source we used a low-pressure inert gas condensation cell. Fullerene vapor from a resistively heated oven was quenched in a helium atmosphere (1–3 mbars) cooled by liquid nitrogen (Fig. 1). The steady helium stream transported the clusters condensed out of the vapor from the condensation cell into a heating cell with a length of 14 cm and 6 mm in diameter. Subsequently, the cluster beam passed through two differential pumping stages into a high-vacuum chamber containing the acceleration region of the TOF spectrometer.

Particularly stable clusters can be identified in a mass spectrum if the clusters are heated to temperatures at which

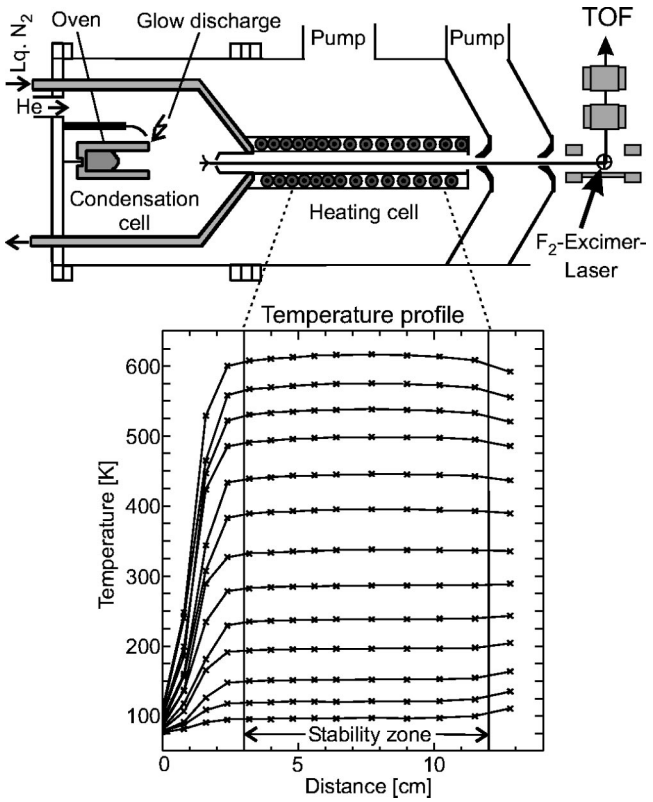

FIG. 1. Experimental setup consisting of the cluster condensation cell, the heating cell, and the TOF spectrometer. For the ionization of the clusters either a laser pulse in the ionization volume or a glow discharge in the condensation cell can be used. The temperature profile of the heating cell, measured with a thermocouple inside the cell, is also shown.

they evaporate molecules. Then the corresponding peaks will appear enhanced in the spectrum. In our former investigation of fullerene clusters[9] heating and ionization were carried out almost simultaneously by laser pulses. Therefore no information about the stability of *neutral* fullerene clusters could be obtained. In contrast, the experimental setup shown in Fig. 1 allows the properties of either charged or neutral clusters to be studied. In the first case, positive and negative cluster ions were formed by a glow discharge inside the condensation cell. After passing through the heating cell one charge species is selected, depending on whether the TOF spectrometer is operated in positive- or negative-ion mode. For the investigation of neutral clusters ionization was accomplished by the light pulse of an F_2 excimer laser (157 nm) after the clusters had passed through the heating cell. Because the photon energy of 7.9 eV is just above the ionization threshold of a C_{60} molecule (ionization potential is 7.6 eV) the clusters can be ionized without additional heating. In a one-photon ionization process the small excess energy is converted to kinetic energy of the electron. Consequently, the intensity anomalies in the resulting mass spectra are indeed reflecting the stabilities of *neutral* $(C_{60})_n$ clusters.

The heating cell is a further development of a design we have used for the investigation of the melting behavior of sodium clusters.[43] As can be seen from Fig. 1, special attention was paid to achieving a constant temperature profile

(± 5 K) over a long distance (stability region ≈ 9 cm). The duration of stay, t_s, of the $(C_{60})_n$ clusters in the stability region was determined experimentally[44] and can be varied between $t_s = 0.5$ ms and 1 ms, depending on the pressure in the condensation cell. From that it can be estimated that the clusters should be well thermalized by at least 10^5 collisions with the helium buffer gas.[45] Even the time the clusters spend in the initial rising region should be sufficient for attaining nearly the plateau temperature. In this manner it is possible to produce a cluster beam with a well-defined temperature in the range between $T_h = 100$ and 700 K.

III. EXPERIMENTAL RESULTS AND DISCUSSION

A. Decay behavior of fullerene dimers

In order to test the functionality of the heating cell, the decay behavior of the *neutral* fullerene dimers $(C_{60})_2$, $(C_{70})_2$, and the singly positively charged dimer $(C_{60})_2^+$ was investigated. Because of the *single* induced dipole-dipole bond the dissociation energy of a dimer lies well below that of the larger fullerene clusters ($n > 2$), where at least *two* ($n = 3$) or *three* ($n = 4$) bonds have to be broken. Therefore the decay of the fullerene dimers occurs in a low-temperature region well separated from that of the trimers and tetramers, which was also checked experimentally. Thus, the dimer population $I_2(T,t)$ can be described by the simple rate equation

$$\frac{d}{dt} I_2(T,t) = -I_2(T,t) k_2(T), \tag{1}$$

where t is the heating time and k_2 the decay rate. Hence, it is possible to investigate the temperature-dependent dimer signal without additional preselection in the experiment. The dissociation energy of a dimer can then be determined directly from the definition equation of the Arrhenius activation energy:[46]

$$D_2 := -k_B \frac{\partial \ln k_2(T)}{\partial (1/T)}. \tag{2}$$

In our experiment the decay rate k_2 was determined from the normalized dimer decay curve $n_2(T,t_s) = I_2(T,t_s)/I_2(100\ \text{K},\ t_s)$:

$$k_2(T) = -\frac{1}{t_s} \ln[n_2(T,t_s)]. \tag{3}$$

As $I_2(T,t_s)$ corresponds to the peak signal of the dimer in the mass spectrum, $n_2(T,t_s)$ represents the surviving probability when the dimer is heated for the time span t_s at the temperature T.[46] Note that according to Eq. (2) the slope of $\ln k_2(T)$ versus 1/T should be independent from t_s as checked experimentally. The value of the activation energy obtained for the neutral dimer $(C_{60})_2$ from the evaluation of several dissociation measurements is

$$D_2[(C_{60})_2] = 0.275 \pm 0.08\ \text{eV}. \tag{4}$$

TABLE I. Binding energies (eV) of the dimers $(C_{60})_2$ ($D_2[(C_{60})_2]$) and $(C_{70})_2$ ($D_2[(C_{70})_2]$) estimated from the cohesion energies of the bulk fullerenes, independently measured by four different groups (Refs. 47–52). As a fullerene molecule in the bulk has 12 nearest neighbors the corresponding dimer dissociation energy D_2 is roughly given by the sixth part of the heat of sublimation $\Delta_{sub} H_m^0$ per molecule. Including non-nearest-neighbor interactions up to the fourth coordination shell causes an additional binding energy in the bulk of about 4% what was considered in the calculated dimer-values.

$D_2[(C_{60})_2]$	$D_2[(C_{70})_2]$	Ref.
0.279 ± 0.009	0.3 ± 0.015	50
0.264 ± 0.007	0.313 ± 0.007	51
0.271 ± 0.035	0.3 ± 0.035	52
0.301 ± 0.004	0.33 ± 0.005	47–49
0.279 ± 0.014	0.311 ± 0.016	Mean value

This value is in good agreement with the one that can be estimated from the cohesion energy of bulk C_{60} (see Table I). Using Eq. (4) the constant C_2 of the Arrhenius law,

$$k_2(D_2,T) = C_2 \exp\left(-\frac{D_2}{k_B T}\right), \tag{5}$$

was determined to be of the order of $C_2 = 4 \times 10^{10}\ \text{s}^{-1}$. Combining the Arrhenius law (5) with the rate equation (1) one gets after time integration a theoretical expression for the surviving probability,

$$n_{2,theo}(T,t_s) = \exp\left[-t_s C_2 \exp\left(-\frac{D_2}{k_B T}\right)\right], \tag{6}$$

which can be compared directly with the experimentally determined values $n_2(T,t_s)$. This is demonstrated in Fig. 2 containing experimental data points $n_2(T,t_s = 0.5\ \text{ms})$ obtained at different temperatures T, as well as the fitted decay curves $n_{2,theo}(T,t_s = 0.5\ \text{ms})$, for the dimers $(C_{60})_2$, $(C_{70})_2$, and $(C_{60})_2^+$. Thereby the dissociation energies of $(C_{70})_2$ and $(C_{60})_2^+$ were determined by fitting Eq. (6) to the experimental data using the same value for C_2 as in the case of $(C_{60})_2$. The resulting dissociation energies are $D_2\ [(C_{70})_2] = 0.313 \pm 0.08$ eV and $D_2\ [(C_{60})_2^+] = 0.372 \pm 0.08$ eV. For the dimer $(C_{70})_2$ the value is in good agreement with that calculated from the cohesion energy of bulk C_{70} listed in Table I.

In the case of the singly charged dimer $(C_{60})_2^+$ the *additional* charge-dipole interaction energy $\Delta D_2[(C_{60})_2^+]$ induced by the charge placed on one of the C_{60} molecules can simply be estimated. Under the assumption that the charge is in time average smeared out over the entire C_{60} surface, the electrical field $\vec{E}(r)$ corresponds to that of a point charge. The interaction energy is then given by

$$\Delta D_2 = -\vec{p}_{ind}\vec{E} = -\alpha_{C_{60}} \vec{E}^2, \tag{7}$$

where $\vec{p}_{ind}$ is the induced dipole moment and $\alpha_{C_{60}}$ the polarizability of the C_{60} molecule. Using the value for $\alpha_{C_{60}}$ recently determined by Antoine *et al.*[31,53] ($\alpha_{C_{60}} = 76.5\ \text{Å}^3$)

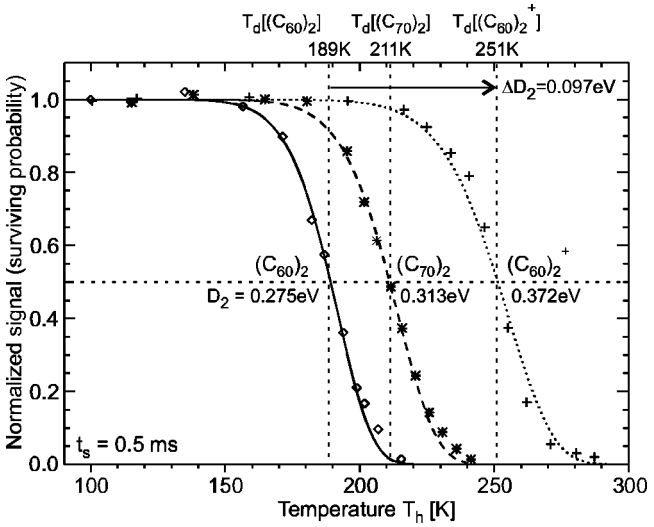

FIG. 2. Comparison between the experimentally determined decay points $n_2(T,t_s=0.5\ \text{ms})$ of the dimers $(C_{60})_2$ ($\diamond$), $(C_{70})_2$ (*), and $(C_{60})_2^+$ (+) and the corresponding fitted decay curves according to Eq. (6) [$(C_{60})_2$, solid line; $(C_{70})_2$, dashed line; $(C_{60})_2^+$, pointed line]. At the top of the diagram the decay temperatures T_d at which the corresponding signal has decreased to $n_2(T,t_s=0.5\ \text{ms})=1/2$ are indicated.

and the equilibrium distance $r=r_0$ for two C_{60} molecules from the PPR potential[14] ($r_0=10.018$ Å) one gets an additional binding-energy contribution of $\Delta D_{2,theo}=0.109$ eV. This value is close to the experimentally observed shift in dissociation energy of $\Delta D_2=0.097$ eV (see Fig. 2).

The experimental data points in Fig. 2 are recorded at a dwell time t_s in the heating cell of 0.5 ms. When the heating time is increased the decay temperatures T_d shift as expected to lower values. When, for example, the dimer $(C_{60})_2$ is heated for $t_s=1.0$ ms, according to Eq. (6) the decay temperature should shift from $T_d[(C_{60})_2]=189$ K down to $T_d[(C_{60})_2]=181$ K. This behavior is indeed confirmed by the experiment (not shown). In principle, a decay occurs at any nonzero temperature, if the heating time t_s is long enough.

The overall picture of the results gained for the simple dimer systems indicates that the heating cell operates as expected. To the best of our knowledge no other gas phase measurements of the dissociation energies of fullerene dimers have been performed so far. The experimentally determined values summarized in Table II are in reasonably good agreement with the bulk values of Table I, and within the estimated values according to Eq. (7).

B. The structure of large $(C_{60})_n$ clusters

One main result of the preceding section was that the binding energy of the charged dimer $(C_{60})_2^+$ is enhanced by about 35% compared to the neutral value. This leads to the initial question as to whether the structure of large $(C_{60})_n$ clusters is also affected by the cluster charge. The answer can be seen in Fig. 3. The enhanced peaks in Fig. 3(b) are the result of heating neutral $(C_{60})_n$ clusters at $T_h=490$ K for $t_s=0.5$ ms. A comparison with the upper and lower part of Fig. 3, containing the intensity anomalies of (a) negatively and (c) positively charged $(C_{60})_n$ clusters heated at the same temperature, shows that the prominent peaks in all three spectra are the same. This clearly indicates that the structure of $(C_{60})_n$ clusters at $T_h=490$ K is *insensitive* to their charge state. Furthermore, mass spectra for negative, positive, and neutral $(C_{60})_n$ clusters were recorded at more than 20 different heating cell temperatures T_h. None of the enhanced peaks at any temperature turned out to be dependent on the charge state $(-/n/+)$ of the cluster. Therefore the result of

TABLE II. Experimental gas phase dissociation energies (eV) of the fullerene dimers $(C_{60})_2$, $(C_{70})_2$, and $(C_{60})_2^+$.

$D_2[(C_{60})_2]$	$D_2[(C_{70})_2]$	$D_2[(C_{60})_2^+]$
0.275 ± 0.08	0.313 ± 0.08	0.372 ± 0.08

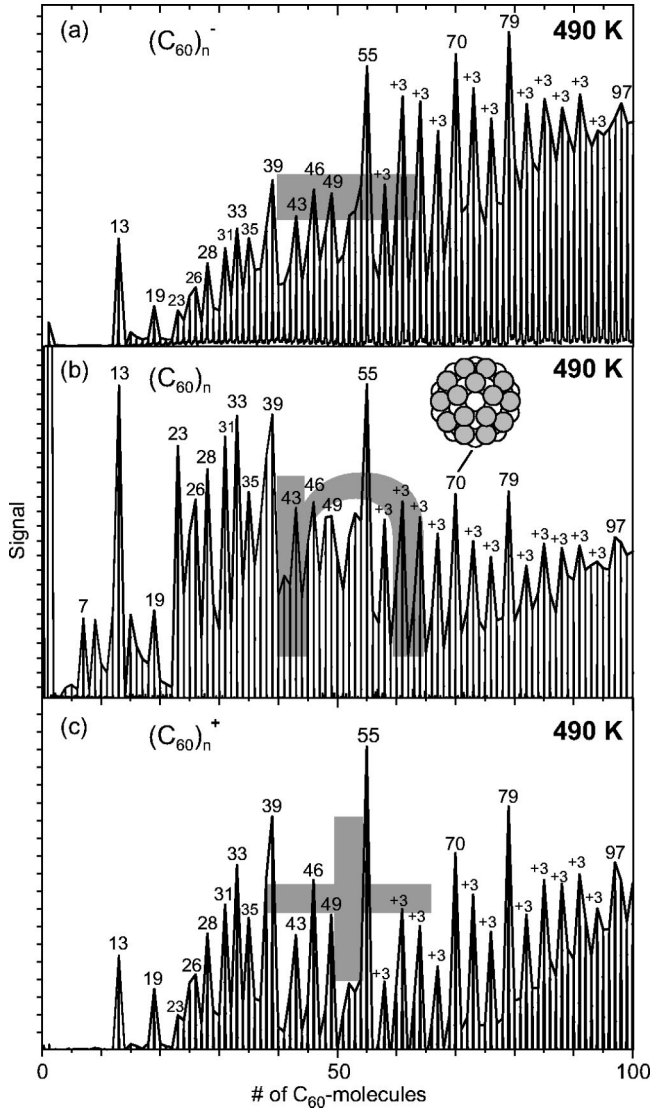

FIG. 3. Mass spectra reflecting the stabilities of (a) negatively, (b) neutral, and (c) positively charged $(C_{60})_n$ clusters at 490 K ($t_s=0.5$ ms). The set of magic numbers of all *three* spectra is identical. Different intensities in individual peaks merely reflect different initial cluster distributions, but have no significance.

charge insensitivity can be generalized to the whole temperature region investigated in this work.

Figure 4 shows mass spectra of $(C_{60})_n$ clusters obtained at four *different* heating cell temperatures at the same heating time $t_s = 0.5$ ms. The size distribution of cold clusters, as grown at $T_h = 100$ K in Fig. 4 (a), is smooth and therefore contains no structural information.

In Fig. 4(b) again a mass spectrum recorded at $T_h = 490$ K is shown, but now in a somewhat larger mass range. Summarizing the 490 K spectra of Figures 3 and 4(b) they can be characterized by a set of unusually strong mass peaks, namely, $n = 13, 19, 23, 26, 28, 31, 33, 35, 39, 43, 49, 55, 55+3m$, 116, 125, 131, 137, and 147 ($m = 1-14$). These, in the cluster literature so-called ''magic numbers,'' are nearly identical to those obtained in our earlier laser heating experiment.[9] Exceptions in the new experiment are found only for the enhanced peaks at $n = 26, 28, 31$, and 33.

When the temperature of the heating cell is further increased the icosahedral magic numbers begin to disappear and other unusually strong mass peaks arise. Finally, the spectrum is dominated by a completely new set of magic numbers. This can be seen in Fig. 4(c) where a $(C_{60})_n$ spectrum recorded at $T_h = 585$ K is shown. The *new* set of magic numbers is $n = 38, 48, 58, 61, 64, 68, 71, 75, 77, 84, 89, 91, 96$, and 98. The enhanced peaks which remained unchanged are located in the low-mass region, namely, $n = 13, 19, 26, 28, 31, 33$, and 35.

Concerning the temperature dependence of the intensity anomalies in the $(C_{60})_n$ spectra, two main questions arise. First, which structures are represented by the different sets of magic numbers? Second, what is the *reason* for the observed temperature dependence? Because the second question can hardly be answered without clarifying the first one we will first of all focus on the structure analysis.

The magic numbers in the 490 K spectra [Figs. 3 and 4(b)] are very similar to those observed for argon and xenon clusters[54,55] — similar but not identical. However, the Lennard-Jones (LJ) potential, by which the interatomic interaction and the occurrence of icosahedral structures in rare-gas clusters can be explained, is not suitable for the description of $(C_{60})_n$ clusters. As already mentioned, these require a potential that is ''harder'' and shorter in range than the LJ potential. Nevertheless, the appearance of icosahedral structures for $(C_{60})_n$ clusters can also be justified just by geometrical arguments.

The strong mass peaks at $n = 13, 55$, and 147 are very suggestive, as they correspond to the number of C_{60} molecules that are necessary to complete the first three shells in the sequence of Mackay icosahedra. However, this conclusion is far from definite since there are two other types of structures with major shell closings for these numbers — cuboctahedra and square-faced truncated decahedra. It is important to make this distinction, since a cuboctahedron of any size can be cut out of a C_{60} fcc-bulk crystal, while icosahedra and decahedra are not consistent with the translational symmetry due to their fivefold symmetry axes. In this sense they are noncrystalline.

When, however, the subshell structure between the major shell closings is considered, cuboctahedra and decahedra can

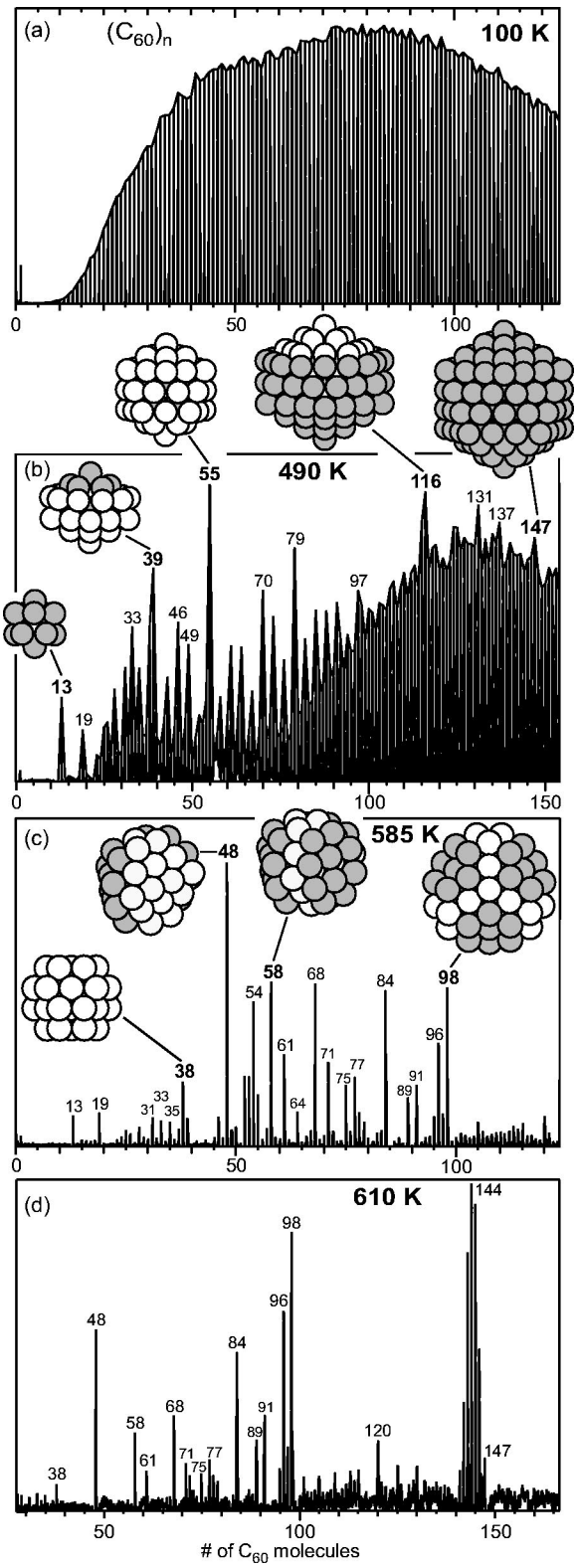

FIG. 4. Mass spectra of $(C_{60})_n$ clusters recorded at heating cell temperatures of (a) 100 K, (b) 490 K, (c) 585 K, and (d) 610 K ($t_s = 0.5$ ms). Representative structures are shown in (b) and (c), where each C_{60} molecule is represented by a sphere. The structures obtained after heating up to 490 K (b) have an icosahedral motif, those obtained after more intense heating (c), (d) are instead close-packed, decahedral, or tetrahedral (see text).

be ruled out. The removal of one triangular face from perfect icosahedral $(C_{60})_n$ clusters containing 55 and 147 molecules yields clusters with 49 and 137 molecules, respectively. The removal of two, three, and five faces yields $n=46, 43, 39$, and 131, 125, 116, respectively. All of these eight numbers are represented by strong peaks in the 490 K spectra. This suggests plausible structures for clusters somewhat smaller than perfect Mackay icosahedra. The magic numbers for clusters with *low* coverage of a complete icosahedral core can be explained by the addition of triangular faces according to the findings of Farges *et al.*[56] and Northby.[57] Hereafter there are two mutually exclusive lattices for the coverage of a closed-shell icosahedron, called IC and FC. The IC lattice consists of all sites of the next larger Mackay icosahedron and is preferred for high coverage, resulting in the magic numbers explained above. For low coverage the IC lattice is energetically disfavored, since the molecules of the new shell have contact with only two molecules of the core. In this case FC sites are preferred, where additional molecules are sitting in a trough built of three core molecules. In particular, for the coverage of the 13-molecule icosahedron the cluster sizes $n=19$, 23, and 26 are favorable fillings of the FC lattice which are also reflected by enhanced peaks in the 490 K spectra. Even more pronounced in the 490 K spectra is the FC sequence based on the 55-molecule icosahedral core. In this case each of the 20 triangular faces of the icosahedron has three FC sites. Thus, the series of unusually strong peaks for the sizes $n=55+3m(m=1-14)$ can be explained by the filling of FC sites on successive triangular faces. Further support for this assumption is given by the mass peaks of $(C_{60})_{70}$ and $(C_{60})_{79}$, which stand out within the $(55+3m)$ series and correspond to the completion of one [cf. Fig. 3(b)], two ''umbrellas'' respectively, around adjacent fivefold axes of the 55-icosahedron.

Finishing the analysis of the 490 K spectra it is worth mentioning that all observed magic numbers which *cannot* be explained by stable icosahedral structures ($n=28, 31, 33$) are located in the intermediate region between FC and IC growth. In this size regime the icosahedral symmetry is not so distinct as in the vicinity of closed shells. Even for LJ clusters the icosahedral structures of the corresponding cluster sizes are only slightly lower in energy than the optimal decahedral structures.[58]

The interpretation of the magic numbers in the 585 K spectrum of Fig. 4(c) is more difficult because no inclusive superior structural motif, as in the case of the icosahedra, could be found. For this reason support from theoretical structural calculations is necessary in order to make reliable conclusions. In a recent work the structure of $(C_{60})_n$ clusters has been modeled by the PPR potential. By means of that, the appearance of nearly all magic numbers in the high-temperature spectra could be explained.[28] The 38-molecule cuboctahedron, as well as the decahedral structure of $(C_{60})_{48}$ shown in Fig. 4(c) represent the global energy minima for PPR clusters and are also predicted to be especially stable. Furthermore, the enhanced peaks in the 585 K mass spectrum occurring at $n=64$, 71, and 75 can be explained by

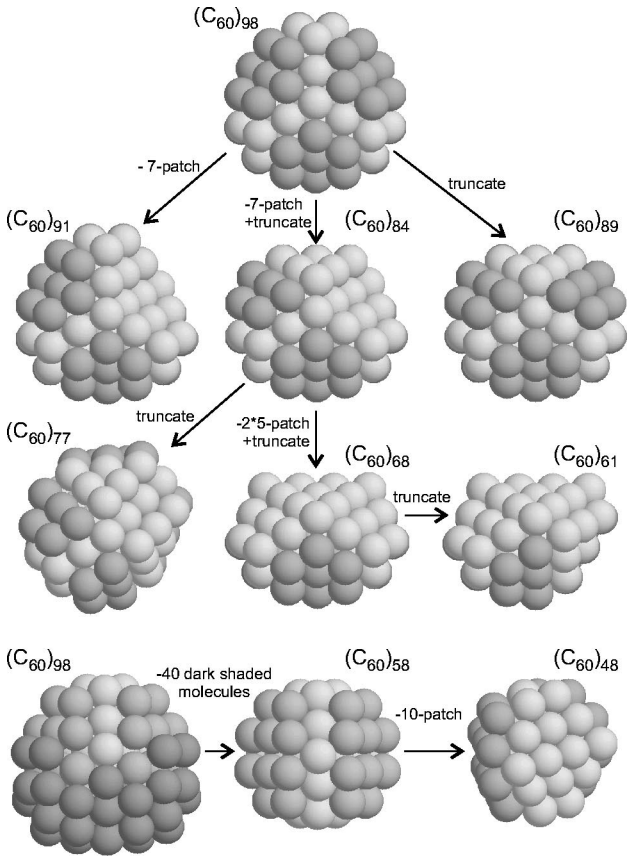

FIG. 5. Particularly stable clusters, based on the 98-Leary tetrahedron, whose peaks are observed as magic numbers in the high-temperature $(C_{60})_n$ spectra. Each C_{60} molecule is represented by a sphere with a diameter corresponding to the equilibrium pair separation. The structures are obtained by the removal of 7-patches from $(C_{60})_{98}$ and/or truncation. The lower part shows in which way the structures of $(C_{60})_{58}$ and $(C_{60})_{48}$ are contained within $(C_{60})_{98}$.

structures based on the 75-Marks decahedron[59] and the peaks at $n=31$, 33, and 35 are most probably due to small decahedra.

A cluster with a quite unusual symmetry, the recently discovered 98-Leary tetrahedron, represents almost certainly the basis for the series of strong peaks at $n=61, 68, 77, 84, 91, 96$, and 98. Thereby it should be noted that these structures do *not* represent the global minima for PPR clusters. However, the energy gap to the optimal structures is rather small ($\approx 0.1-1$ eV) compared with the huge energy difference to the icosahedral configurations ($\approx 1-3.3$ eV).[28] When the structures are restricted to those derived from the Leary tetrahedron, the above magic numbers are perfectly reflected in a theoretical energy difference spectrum of the corresponding PPR clusters.[28] Hence, our initial interpretation of these magic numbers, based only on geometrical arguments,[32] is confirmed. Figure 5 illustrates how the especially stable structures can be cut out of the 98-Leary tetrahedron. The latter consists of a 56-molecule stellated fcc-based tetrahedron (bright spheres), whose six faces are each covered by hexagonal arrangements consisting of seven molecules (darker spheres). If one of these 7-patches is removed, the result is a stable structure with a

total of 91 molecules. Also the strong peaks at $n=89$ and $n=84$ can be explained in a similar way. Truncation at one edge of $(C_{60})_{98}$ by removal of three bright and six dark spheres leads to a quite compact cluster with a total of 89 molecules. The structure of $(C_{60})_{84}$ is obtained by the removal of one 7-patch and additional truncation. Continuing this procedure further reveals the configurations of $(C_{60})_{68}$ and $(C_{60})_{61}$. Finally, the structure of $(C_{60})_{77}$ can be derived from $(C_{60})_{91}$ by truncation at the two adjacent edges of the missing 7-patch. Additionally, it is shown in Fig. 5, in which way the structures of $(C_{60})_{58}$ and $(C_{60})_{48}$ are contained within the Leary tetrahedron. Thus, the structural family of clusters based on the 98-tetrahedron can be extended to these two configurations. Hence, the Leary tetrahedron appears to represent the dominating structural motif in the high-temperature spectra.

The reason why the strong peak at $n=54$ in Fig. 4(c) was excluded from the list of magic numbers is that the peaks between $n=52$ and 54 are remainders from the stable 55-icosahedron. The molecules at the vertices of the icosahedron are poorly bound to the layer underneath because they are only in contact with one core molecule. Therefore, the bundle of peaks at $n=52-54$ corresponds to icosahedra with missing vertex molecules. Evidence is given by the fact that these peaks disappear when the temperature is slightly increased. This is already the case in the spectrum shown in Fig. 4(d), which was recorded at $T_h=610$ K. In contrast to the other prominent features in the spectrum, the peaks associated with the 55-icosahedron in the region $n=52-55$ vanished. This finding is also important for the interpretation of the prominent peaks at $n=58$ and 61. It indicates that they are no longer based on the 55-icosahedron, but represent new structures. In analogy, the peaks between $n=141$ and 146 in the high mass region of the spectrum in Fig. 4(d) represent missing vertex molecules of the 147-icosahedron.

So far we have shown that $(C_{60})_n$ clusters heated up to 610 K for $t_s=0.5$ ms adopt different structures. However, we have not discussed the reasons for the occurrence of the two structural phases. In principle, there are three possible explanations for the observed effect.

First, the spectra recorded at the different temperatures could reflect the thermodynamically most stable structures. For nonzero temperatures not the potential energy E, but the free energy $F=E-TS$ (T, temperature; S, entropy) is the relevant thermodynamical variable for the determination of the preferred equilibrium structures. Since the icosahedral structures definitely do *not* represent the global energy minima (at $T=0$ K) and are also considerably higher in potential energy than, for example, the tetrahedral structures,[28] they would only be preferred at *high* temperatures because of their larger vibrational entropy.[28,39] Consequently, this kind of equilibrium solid-solid transition, which was observed in some systems as a premelting effect,[34–37] is most probably not responsible for the structural change in $(C_{60})_n$ clusters in the investigated temperature range.

A second possible explanation has recently been suggested by Baletto *et al.*[41] They assume that besides preformed icosahedral configurations also a small amount of close-packed decahedral and tetrahedral structures could be formed in the inert gas condensation cell. When heating to high temperatures the less stable icosahedral structures would decay while the more stable nonicosahedral clusters would survive and are observed. We cannot exclude this possibility directly from our experimental data, because the total cluster signal decreases continuously with increasing temperature due to diffusive losses at the walls and the exit of the heating cell. Therefore, only the relative stability of large clusters can be investigated. However, the dissociation energies, i.e., the energy required to remove the most weakly bound molecule, are only slightly different for the tetrahedral structures and, for instance, the icosahedral structure of $(C_{60})_{55}$ ($\Delta E<0.09$ eV, PPR potential). Furthermore, in Fig. 4(d) the strong peak of $(C_{60})_{98}$ and residual peaks of the $(C_{60})_{147}$-icosahedron are simultaneously present. But when the temperature is further increased, the peak of $(C_{60})_{98}$ disappears before those belonging to the 147-icosahedron do, although the dissociation energy of $(C_{60})_{147}$ and its fragments is ca. 0.35 eV lower than that of $(C_{60})_{98}$. Moreover, according to the growth simulations of Baletto and coworkers the formation of nonicosahedral structures were observed only at relatively high growth temperatures (525–550 K). In our experiment, however, the $(C_{60})_n$ clusters grow in a condensation cell with a surrounding helium gas temperature of about 80 K (Fig. 1). The binding energy per C_{60} molecule in a $(C_{60})_n$ cluster is rather weak and there exist a great number of internal degrees of freedom, $(180n\text{-}6)$, due to intermolecular vibrations $(3n\text{-}6)$, intramolecular vibrations $(171n+6)$, and rotations $(6n\text{-}6)$ to which the internal energy can be distributed. As the clusters stay, in general, for several milliseconds in the condensation cell, there is enough time to redistribute the condensation energy to the internal degrees of freedom.[60] Therefore only a moderate increase of temperature is expected during the growth process as a result of the heat of adsorption of newly bonded molecules. *Without* cooling the maximum temperature of a cluster that is reached after growth can be estimated from the total binding energy. The temperature of $(C_{60})_{55}$, for instance, should be of the order of 400 K, when the contributions from the intramolecular vibrations are weighted corresponding to their Einstein functions. However, depending on how fast the heat exchange with the atoms of the cold helium buffer gas occurs, the real growth temperature in the condensation cell is expected to be considerably lower. Thus, the most likely scenario is that depending on the growth temperature, the $(C_{60})_n$ clusters are either completely disordered or icosahedra with some disorder left. The amount of disorder will increase with decreasing growth temperature.[41] Subsequent moderate heating then would lead to kinetical trapping in the perfect icosahedral configurations observed in the 490 K spectra. Remarkably, the icosahedral structures represent neither the global minima of potential energy nor those of the free energy at this given temperature.[41]

Therefore, the third and most plausible explanation for the two structural phases reflected in the $(C_{60})_n$ spectra is a transition from *metastable* nonequilibrium icosahedral to the close-packed decahedral and tetrahedral equilibrium structures presumably lowest in free energy at this temperature.

Thus, it seems that with the structural transition, thermodynamical equilibrium has been established on the experimental time scale.

How can one imagine the trapping of the cluster structure in a metastable state? Doye and co-workers have introduced a terminology for characterizing potential energy surfaces (PES's) of clusters that can give important clues towards the understanding of the kinetics and thermodynamics in these small systems.[58,61,62] A PES can, for example, be characterized as having a single funnel, a double funnel, or even a multiple funnel landscape. This can be visualized in so-called disconnectivity graphs in which a set of low-lying local minima and transition states are mapped. If a cluster has a single funnel landscape, as is the case for most LJ clusters, the PES is dominated by one large basin with the global energy minimum at its bottom. Hence, the optimal structure for LJ clusters is usually easy to find, because there is a superior downhill force towards the global minimum. Exceptions from this relatively simple case are the LJ clusters LJ_{38}, LJ_{75}-LJ_{77}, and LJ_{98}, whose PES's have a double funnel landscape.[33,58,61] This causes a completely different thermodynamic behavior. The funnel leading to the global minimum (namely, the 38-cuboctahedron, the 75-Marks decahedron, and the 98-Leary tetrahedron) is deep but narrow and therefore difficult to find. The funnel leading to the icosahedral structures is broad, i.e., easy to find. Furthermore, the structural similarity between icosahedral and disordered structures is much greater than between disordered and, for example, closed-packed structures.[63] This gives a topological argument for the higher accessibility of the icosahedral structure region from the disordered state. For these reasons trapping in the icosahedral funnel is much more likely than the direct relaxation to the global minimum structure.

When the potential becomes harder and shorter in range, as is the case for $(C_{60})_n$ clusters, the PES becomes more flat and rugged.[64] Therefore, in general, the number of funnels increases. Nevertheless the growth simulations of Baletto and co-workers show that trapping in icosahedral structures is still preferred, although they are thermodynamically much less favorable than for LJ clusters.[28,41] For such sticky potentials structural rearrangements are more difficult to achieve[65] because the *local* potential barriers become sharper and higher.[64] Furthermore, there are large interfunnel barriers evident on the PES of $(C_{60})_n$ clusters,[28] additionally indicating the difficulty of major structural transformations. Thus, if the structure is once trapped in a metastable structural region, it is expected to take a relatively long time and/or requires high temperatures to escape.

In order to quantify the dependence of structural transitions and decay processes in $(C_{60})_n$ clusters on heating time and temperature in greater detail, we focused on the behavior of selected cluster sizes. For this purpose mass spectra were recorded in sequences of small temperature steps. Afterwards the temperature-dependent ratios of selected peak values were calculated. An example using this method is shown in Fig. 6 (a). Here the decay behavior of $(C_{60})_{55}$ on the basis of the peak ratios $(C_{60})_{56}/(C_{60})_{55}$, $(C_{60})_{55}/(C_{60})_{54}$, and $(C_{60})_{54}/(C_{60})_{53}$ was investigated. At temperatures lower than

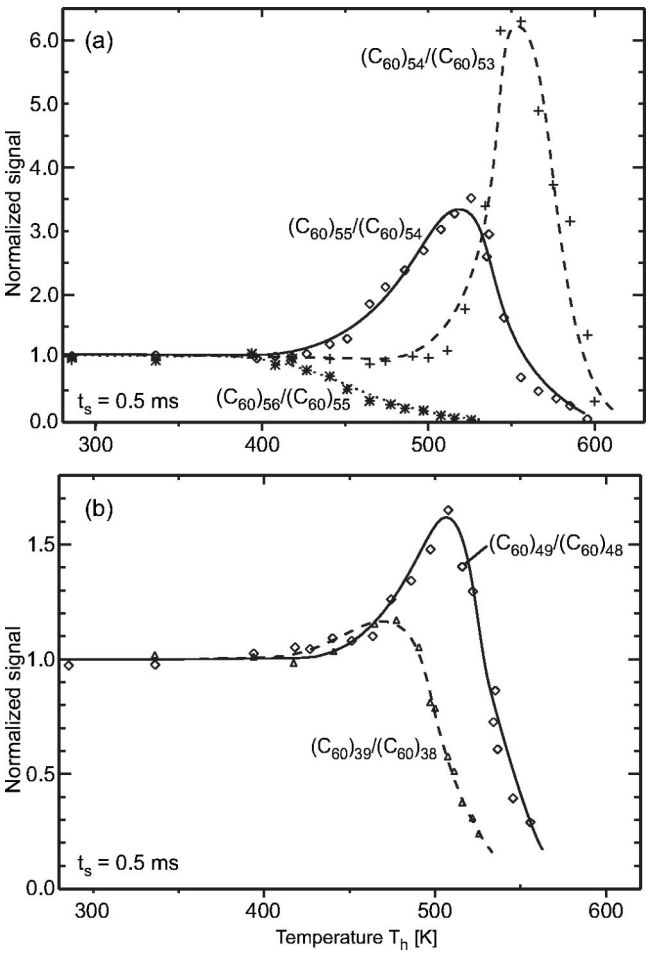

FIG. 6. (a) Dependence of the experimentally determined peak ratios $(C_{60})_{56}/(C_{60})_{55}$ (*), $(C_{60})_{55}/(C_{60})_{54}$ ($\diamond$), and $(C_{60})_{54}/(C_{60})_{53}$ (+) on the heating cell temperature T_h ($t_s = 0.5$ ms). (b) Dependence of the experimentally determined values of $(C_{60})_{39}/(C_{60})_{38}$ ($\triangle$) and $(C_{60})_{49}/(C_{60})_{48}$ ($\diamond$) on the temperature T_h ($t_s = 0.5$ ms). The fitted curves in (a) and (b) are only to guide the eye.

$T_h = 400$ K all ratios are, as expected, equal to 1. When the temperature is increased above 400 K, the peak ratio $(C_{60})_{56}/(C_{60})_{55}$ decreases monotonically due to the great difference in stability between these two clusters. In contrast, the value of the ratio $(C_{60})_{55}/(C_{60})_{54}$ first increases because $(C_{60})_{55}$ emerges as a magic cluster. However, at temperatures above $T_h = 500$ K the probability that one vertex molecule is evaporated becomes significant and thus the ratio decreases. The evaporation of one vertex molecule is also reflected in the ratio $(C_{60})_{54}/(C_{60})_{53}$ that rises in the temperature region between $T_h = 500$ K and ca. 560 K. The subsequent decrease indicates the loss of a second vertex molecule. In this manner it is possible to monitor the temperature dependence of the successive loss of one and two C_{60} molecules from the closed-shell 55-icosahedron prior to the complete decay.

In a similar way the temperature dependence of the structural transition can be investigated. For this purpose it would be favorable to find neighboring peak-pairs each representing a prominent icosahedral and close-packed (decahedral or tetrahedral) structure. For this reason we have selected the peak

ratios $(C_{60})_{39}/(C_{60})_{38}$ and $(C_{60})_{49}/(C_{60})_{48}$ as suitable candidates for investigation. For $(C_{60})_{39}$ the optimal icosahedral structure is an especially stable half-shell closing [Fig. 3(b)]. For $(C_{60})_{38}$ the global energy minimum is represented by the 38-cuboctahedron. Similarly, for $(C_{60})_{49}$ the lowest-energy icosahedral structure is a subshell closing and in the case of $(C_{60})_{48}$ the global minimum is the particularly stable decahedral structure shown in Fig. 5.

In Fig. 6 (b) the temperature dependence of the peak ratio $(C_{60})_{49}/(C_{60})_{48}$ is presented. Below $T_h = 400$ K the ratio takes again the value 1. With increasing temperature the ratio increases due to the emerging icosahedral subshell closing of $(C_{60})_{49}$ against the relatively unstable structure of $(C_{60})_{48}$, which in this temperature region is also expected to be icosahedral. The maximum value of the ratio is reached at about 510 K, followed by a rapid decrease. This decrease signals the occurrence of the transition towards the high-temperature decahedral structure. Remarkably, within a temperature span of about 50 K the absolute value of $(C_{60})_{49}/(C_{60})_{48}$ switches from ca. 1.7 to 0.3, which indicates a complete reversal of the stability ratio. An analogous temperature evolution is also observed for the peak ratio $(C_{60})_{39}/(C_{60})_{38}$. In this case the rise (values greater than 1) is not so steep as for $(C_{60})_{49}/(C_{60})_{48}$ and the transition to the close packed is shifted by about 30 K to lower temperature [Fig. 6(b)]. This fits to the general trend that higher temperatures are needed to cause a structural transition in larger clusters. A similar size dependence was already observed in the melting behavior of sodium clusters.[43] However, in each individual case the topology of the PES plays an important role and therefore the transition temperatures can locally fluctuate. For example, the barrier height between the different structural regions and the length of the transition path vary from cluster to cluster.[58,63] Because the dimension of the configuration space increases as $3n-6$, it is expected that, in general, the lengths of the transition paths also get longer and therefore higher temperatures and/or longer heating times are required to reach the thermodynamical equilibrium state. In this context we have investigated the correlation with temperature and heating time experimentally using the smallest and the largest clusters for which a structural transition could be observed, namely, the clusters $(C_{60})_{38}$ and $(C_{60})_{98}$. In Fig. 7 the peak ratios $(C_{60})_{37}/(C_{60})_{38}$ and $(C_{60})_{99}/(C_{60})_{98}$ are plotted versus the heating cell temperature for two *different* heating times $t_s = 0.5$ ms and 1.0 ms. These two ratios are composed of an especially stable high-temperature structure (38-cuboctahedron, 98-Leary tetrahedron) and a cluster that is neither especially stable nor particularly unstable in the icosahedral and the high-temperature structural phase. Hence, with increasing temperature a monotonic decrease is expected and observed for both peak ratios. The decline of the curves can be interpreted as a disappearance of the icosahedral structures and emergence of the corresponding high-temperature structures.

Although a theoretical description of such an interfunnel transition does not seem to be possible in a simple way, Miller *et al.* have recently demonstrated that the icosahedral-fcc interfunnel transition in LJ_{38} obeys an Arrhenius law.[66] Therefore, we have fitted an Arrhenius decay curve, Eq. (6),

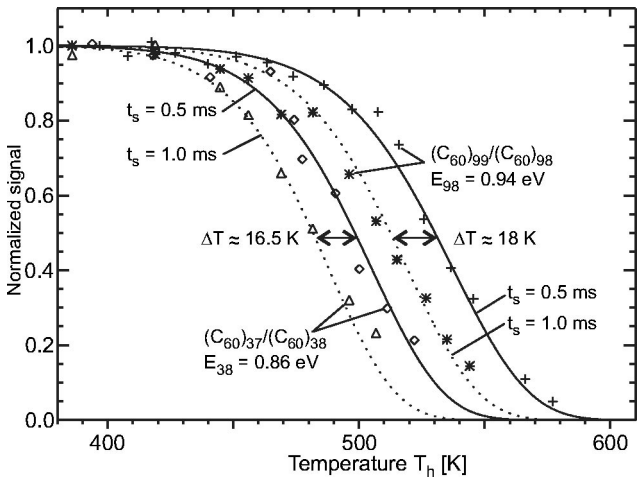

FIG. 7. Experimentally determined values of the peak ratios $(C_{60})_{37}/(C_{60})_{38}$ and $(C_{60})_{99}/(C_{60})_{98}$ recorded at two different heating times: (1) $t_s = 0.5$ ms ($\diamond$, 37/38; +, 99/98), (2) $t_s = 1.0$ ms ($\triangle$, 37/38; *, 99/98). The fitted curves correspond to Eq. (6) for $t_s = 0.5$ ms (solid lines) and $t_s = 1.0$ ms (dotted lines).

to the experimental data points in order to get a quantitative estimate of the temperature- and time-dependent behavior. However, it has to be emphasized that in this way an Arrhenius-like interfunnel behavior cannot be proved for $(C_{60})_n$ clusters. For the Arrhenius constant C_n we used the value obtained for the dimer $(C_{60})_2$ multiplied with the size-dependent factor $n^{2/3}$ that considers the effective surface for rearrangement steps. In this manner the values for the formal Arrhenius activation energies E_n [D_2 in Eq. (6)] are found to be $E_{38} = 0.86$ eV and $E_{98} = 0.94$ eV. For comparison, the value obtained for the Arrhenius activation energy of the icosahedral to fcc transition in LJ_{38} is E_{38} (LJ) $= 3.19\varepsilon$.[66] With the C_{60} pair well depth of $\varepsilon = 0.275$ eV [Eq. (4)] this corresponds to $E_{38}(\mathrm{LJ}) = 0.877$ eV.

Furthermore, the temperature shift expected from Eq. (6) due to the longer heating time of $t_s = 1.0$ ms (dotted lines) fits well with the corresponding measured values of the peak ratios $(C_{60})_{37}/(C_{60})_{38}$ ($\triangle$) and $(C_{60})_{99}/(C_{60})_{98}$ (*). The expected [(Eq. 6)] and observed temperature shifts are $\Delta T \approx 16.5$ K for the peak ratio $(C_{60})_{37}/(C_{60})_{38}$ and $\Delta T \approx 18$ K in the case of $(C_{60})_{99}/(C_{60})_{98}$. This illustrates how the temperature required for attaining the high-temperature structures is lowered with increasing heating time.

IV. THEORETICAL RESULTS

It has to be pointed out that the clusters ultimately belonging to a magic number peak in the mass spectrum originate from larger clusters which have lost a large number of molecules by evaporation. Therefore the measured temperature dependencies could be distorted by ensemble effects. The ideal computational support for the performed experiments would therefore be a molecular dynamics (MD) simulation of the shrinking of a large ensemble (e.g., $n = 1$–200) of originally disordered clusters by multiple evaporation at constant temperature. After a given heating time (e.g., $t_s = 0.5$ ms) the size distribution of the ensemble would be

inspected for magic numbers. However, such a computation is hardly feasible for the long experimental time scales. Therefore we restricted our MD calculations to single cluster sizes and shorter heating times t_{MD}. The purpose of these simulations is to give some hints how the temperature dependence of the icosahedral and nonicosahedral structures can be explained.

In order to conserve the cluster size we placed the clusters in a box with a size of $80\times80\times80$ Å^3, whose reflecting walls prevented the molecules from evaporating. Furthermore, this box roughly simulates the situation within a hot evaporating ensemble in which the clusters continuously decay by evaporation and are generated by the decay of larger clusters. This situation is approximated by the evaporation and back bouncing of the molecules from the container walls. In the MD simulations the intermolecular C_{60} interaction was modeled by the two-body PPR potential, as well as by a Morse potential[67] V_M:

$$V_M=\varepsilon\{e^{\rho(1-r/r_0)}[e^{\rho(1-r/r_0)}-2]\}. \tag{8}$$

Here ε is the pair well depth, r_0 the equilibrium pair separation, and ρ the so-called range parameter. Such spherical potentials should be an appropriate description for the bonding conditions in $(C_{60})_n$ clusters, since the C_{60} molecules rotate freely even at relatively low temperatures.[68]

In relation to the experiments for single cluster sizes presented in Fig. 6(b), we selected cluster sizes with particularly stable decahedral and close-packed structures, namely, $n=48$ and 38, for the simulations. Because of the significant energy differences to the icosahedral configurations, the occurrence of a structural transition can be identified very easily. All MD simulations were started from completely random cluster configurations. The temperature T was held constant by means of an Andersen thermostat.[69] We used a velocity Verlet algorithm with a time step of $dt=20$ fs. We checked that the results remain unchanged when using shorter time steps *dt*, obtained in selected MD runs with $dt=10$ fs and 5 fs.

Information about the current cluster structure and the associated potential energy values were obtained during the simulations by systematic quenching every 1–10 ns. In Fig. 8 the time evolution of the potential energy for a 48-Pacheco-Prates-Ramalho-cluster (PPR_{48}) heated to 750 K is shown. The total heating time was $t_{MD}=10$ μs. Starting from disordered configurations the cluster structure developed after ca. 0.5 μs into the icosahedral region (funnel). This can be seen from the sharp lower edge in potential energy at $E_{ico}=194.43\varepsilon_{PPR}$. This energy value corresponds to the lowest-energy icosahedral structure. The other energy values within the icosahedral region represent suboptimal icosahedral structural isomers. In this simulation the cluster structure stayed in the icosahedral funnel for more than 5 μs, before the free energy barrier to the structural region of the decahedral global minimum ($E_{glob}=197.904\varepsilon_{PPR}$) was finally overcome. This MD run demonstrates that a $(C_{60})_n$ cluster can indeed be trapped for a relatively long time span in the metastable icosahedral region even at a high temperature. In order to determine how sensitive this result is

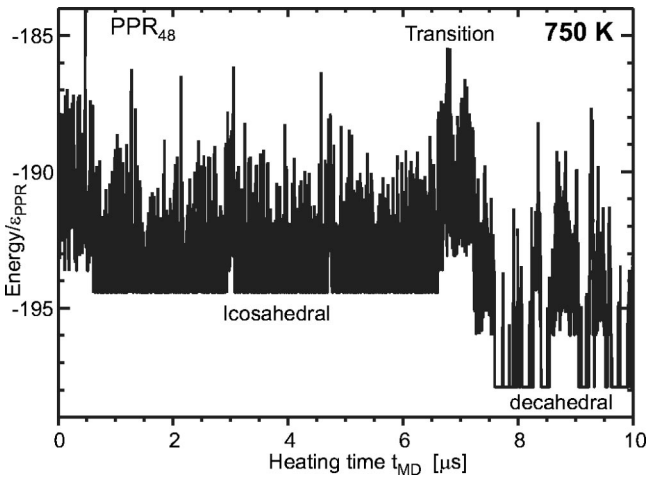

FIG. 8. Time evolution of the potential energy of PPR_{48} during a canonical MD simulation at $T=750$ K. The plotted energy values were obtained after quenches every nanosecond. The energy scale is in units of the PPR pair potential depth $\varepsilon_{PPR}=0.2667$ eV. The simulation was started from a random disordered structure. Thereafter the cluster structure developed first into the icosahedral funnel with the deepest minimum $E_{ico}=197.904\varepsilon_{PPR}$. Here the cluster stayed for ≈6 μs before the global decahedral minimum ($E_{glob}=194.43\varepsilon_{PPR}$) was found.

to the shape of the potential we tested various intermolecular potentials with different range and repulsion in our MD simulations. This can easily be done using the Morse potential (8) with $\varepsilon=0.28$ eV by adjusting the range parameter ρ. With decreasing ρ, the attractive range of the potential increases and the repulsive wall softens. In this way various pair potentials can be fitted by the Morse potential, leading to the same optimal structures and predicted magic numbers.[30] For example, the LJ potential corresponds to a range parameter of $\rho_{LJ}=6.0$, the PPR potential to $\rho_{PPR}=11.28$, and the GF potential to $\rho_{GF}=13.62$. It should be mentioned that the PPR potential already contains a Morse potential.[14]

We did not perform growth simulations, as in the work of Baletto *et al.*,[41] but started the simulations from disordered configurations. Thereby it was noticed that for range parameters larger than ρ_{PPR} the probability that the structure initially develops into close-packed and decahedral structural regions increases. Otherwise, when the range parameter was decreased, the probability for icosahedral structures was increased. For a range parameter between $\rho=10.5$ and 10.8 in about 70–80 % of all performed MD runs, the cluster structure *initially* developed into the icosahedral region. This fits well with the findings from the growth simulations[41] and the experimental low-temperature observations. As the shape of $V_M(\rho=10.8)$ is still very close to the PPR potential, we investigated this type of Morse clusters more extensively. In Fig. 9, representative[70] MD runs for the cluster M_{48} ($\rho=10.8$) at *four* different simulation temperatures for the relatively long heating time of $t_{MD}=100$ μs are shown. In each case the structure initially developed into the icosahedral structural region. In the lowest-temperature simulation performed at $T=575$ K [Fig. 9(a)] the deepest icosahedral minimum ($E_{ico}=188.144\varepsilon$) was reached after a simulation

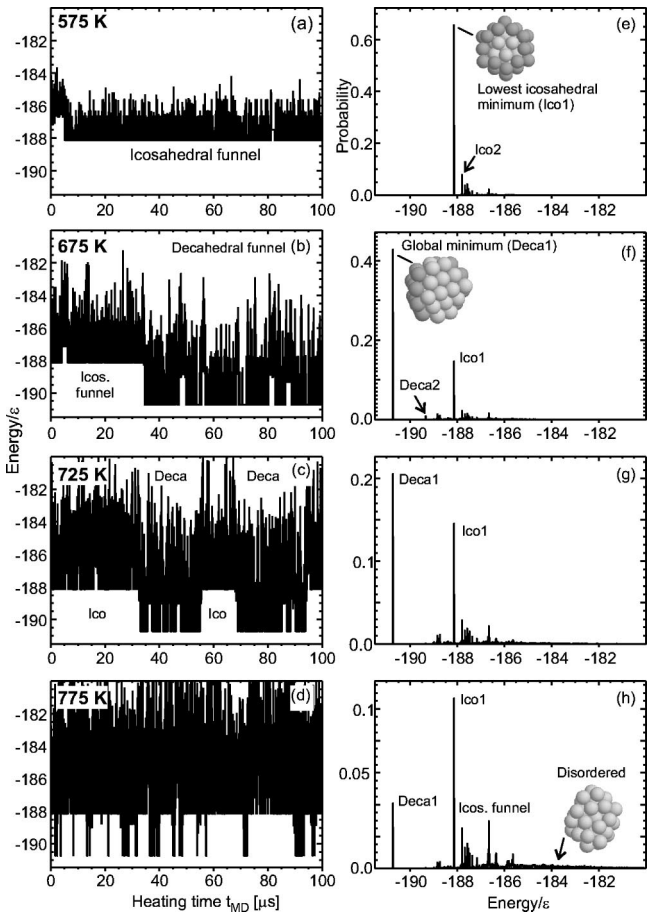

FIG. 9. (a)–(d) Time evolution of the potential energy (quench step: 10 ns) for the Morse cluster M_{48} ($\rho=10.8$) during canonical MD simulations at the temperatures (a) 575 K, (b) 675 K, (c) 725 K, and (d) 775 K. In all MD runs the total heating time was $t_{MD}=100$ μs. (e)–(i) Probability distributions of the potential energies for the corresponding MD runs (a)–(d) in the left column (see text).

time of about 5 μs. For the rest of the simulation (ca. 95 μs) the cluster stayed in the icosahedral funnel, as again seen from the sharp edge in potential energy. Moreover, this is reflected in Fig. 9(e) in which the probability distribution of the potential energy values (structures) is shown. The dominating peak in Fig. 9(e) belongs to the lowest-energy icosahedral isomer of M_{48}. In contrast to that, the icosahedral minimum, second lowest in potential energy (Ico2), has only a minor probability.

Surprisingly, in the $T=675$ K simulation of Fig. 9(b) a transition from the icosahedral to the decahedral funnel containing the global energy minimum ($E_{glob}=190.73\varepsilon$) occurs after a simulation time of 34.7 μs. Afterwards the structure stays in the decahedral funnel until the end of the applied heating time. Thus, in the corresponding probability distribution of Fig. 9(f) now the energy value of the decahedral global minimum has the largest weight. When the temperature in the simulations is further increased to $T=725$ K [Figs. 9(c,g)] and 775 K [Figs. 9(d,h)] the cluster configuration switches more and more between the icosahedral and the decahedral regime. This means that thermodynamical equilibrium between both structural regions is reached on the simulated time scale. Interestingly, in the 775 K simulation the icosahedral structures have again the highest occupation probability. This seems plausible, because at very high temperatures, icosahedral and finally disordered (liquidlike) structures must become lowest in free energy due to the larger entropy contributions.[34–37,39]

With respect to the experiment, the results of the MD simulations from Fig. 9 can be interpreted as follows. The trapping in the metastable icosahedral structural region [Figs. 9(a,e)] corresponds to the situation in the low-temperature 490 K $(C_{60})_n$ spectra. The transition to the high-temperature structures of Figs. 4(c,d) is reflected in the simulations at $T=675$ K and 725 K. In this case at the end of the heating time $t_{MD}=100$ μs, a decahedral configuration would be detected with the highest probability.

As seen, the temperatures required in the MD simulations for the observation of the different structural phases are about 75–100 K higher than the corresponding temperatures in the experiment. This can be explained by the five times shorter time scale ($t_{MD}<1/5t_s$) of the simulation but also by the lack of calculations to describe the processes in a large cluster ensemble.

The transition *back* to icosahedral structures at very high temperatures, as predicted by the MD run at $T=775$ K [Figs. 9(d,h)], could not be observed in the experiment.

We have also performed extensive MD simulations for the 38-molecule cluster M_{38} ($\rho=10.6$) and obtained a very similar temperature behavior for the structure as in Fig. 9 (not shown). The initial transition from the icosahedral funnel to the global fcc minimum was observed at a simulation temperature of $T=650$ K. At this T the 38-cuboctahedron also has the highest probability in the corresponding energy distribution. At temperatures above $T=700$ K icosahedral structures were again preferred as in the case of Fig. 9(h).

It has become clear that the shape of the intermolecular potential plays a crucial role in determining both the optimal structures and the kinetical/thermodynamical behavior of $(C_{60})_n$ clusters. In general, the energy differences between the global minima and the energy values of the lowest icosahedral structures decrease with the increasing range of the potential.[30] Furthermore, the transition size from icosahedral to nonicosahedral structures in small clusters shifts to larger sizes. In this context it is also worth noting that the Morse cluster M_{55} is the only large cluster ($n>20$) with an icosahedral global minimum in the investigated parameter range of $\rho=10.5$–10.8. Therefore *no* structural transition is expected for M_{55} with increasing temperature, in agreement with the experimental observations shown in Figs. 4 and Fig. 6(a). Principally the same is valid for the magic numbers at $n=13$ and 19, the icosahedron and the double icosahedron. Also for these clusters no structural transitions are observed in the experiments with increasing temperature. The double icosahedron becomes the global minimum of M_{19} for $\rho<10.7$. However, at the experimental temperatures the icosahedral structure should become lowest in free energy even for considerably higher range parameters.[28]

Summarizing, it is still uncertain which potential is the most appropriate for $(C_{60})_n$ clusters. Because of the approximations made in the MD simulations it is only possible to

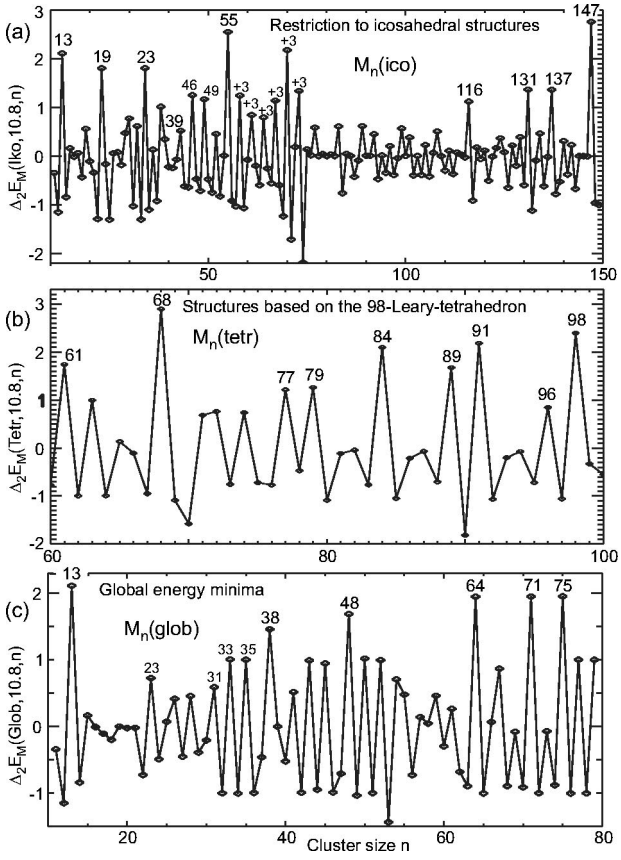

FIG. 10. Simulated magic number spectra for Morse clusters ($\rho=10.8$), by plots of the second energy difference $\Delta_2 E_M = E_M(n+1)+E_M(n-1)-2E_M(n)$. In (a) the cluster structure was restricted to icosahedra, in (b) to a sequence based on the 98-Leary tetrahedron, and in (c) the global minimum energy values were used.

make some very crude conclusions concerning the intermolecular potential. Therefore the simulations have to be seen only as one part in a big mosaic consisting of all the work[13–30,41,65] that has been done in this field. Reviewing the present picture it can be stated that the PPR potential gives a better description of bulk C_{60} than the Girifalco potential, but it could be still too short ranged. For a Morse potential with ρ in the range 10.5–10.8 the equilibrium between the icosahedral and the high-temperature structures seems to be more balanced, which is important for the observation of both structural phases.

Furthermore, it is interesting that the experimental spectra can be well described by an artificial restriction to the different structural phases, as can be seen from Fig. 10. When Morse clusters with $\rho=10.8$ were restricted to icosahedral structures [Fig. 10(a)] nearly all magic numbers of the 490 K spectra were reproduced. The high-temperature magic numbers were found in the simulated spectrum of the 98-Leary tetrahedron sequence [Fig. 10(b)] and in that of the global energy minima [Fig. 10(c)].

V. CONCLUSIONS

In the present work we could give important experimental and theoretical clues towards the understanding of the long-standing discussion on the structure of $(C_{60})_n$ clusters. Beginning with the first results for laser heated $(C_{60})_n$ clusters from the year 1993 (Ref. 9) it seems now clear that the reason for the observed icosahedral structures was kinetic trapping in metastable states due to the very short heating time ($\approx$15 ns). Although in this initial work it was concluded that "It would not have been surprising to have found that C_{60} molecules pack together in clusters as if they were hard spheres."[9] it was not expected that such long tempering times would be required to achieve that goal.

The exact temperature dependence of the structural transition that was measured for selected $(C_{60})_n$ clusters has shown reasonable correlations with the temperature shifts and activation energies expected from a simple Arrhenius model. This experimental information, together with the qualitative results from the molecular dynamics simulations, strongly indicates that the observed change in magic numbers is indeed due to a structural transition from metastable icosahedral structures to configurations that are probably lowest in free energy at the experimental temperature.

However, there are still many open questions and problems to solve. The most important point is the shape of a realistic intermolecular potential. So far no potential has yielded unusually stable global minima for *all* observed high-temperature magic numbers. But this requirement is also not necessary, since these structures only have to be the global minima of free energy at the corresponding high temperatures. Such free energy calculations would however be a very challenging task. At least, the vibrational entropy of the 98-Leary tetrahedron is larger than for the alternative decahedral and close-packed structures and lower than in the case of an icosahedron.[28] Since the potential energy of an icosahedron is however much greater than for the 98-tetrahedron, it seems plausible that there is a temperature window where the tetrahedral structure is stabilized, according to the results from Fig. 9.

Finally, it has to be pointed out that the performed simulations are not able to reproduce the whole complexity of the experiment but can only give some important hints based on a simplified system. Therefore, even though it was possible to simulate the structural transitions of single clusters enclosed in a container, it would still be interesting to compare the results with a simulation of a whole cluster ensemble in order to investigate the effects of combined evaporative shrinking and structural transition.

ACKNOWLEDGMENTS

The authors thank Dr. Jonathan, P. K. Doye, Dr. Erik Koch, and Professor David Tomanek for useful discussions.

*Author to whom correspondence should be adressed. Present address: Max-Planck-Institut für Festkörperforschung, Heisenbergstrasse 1, 70569 Stuttgart, Germany. Email address: n.malinowski@fkf.mpg.de; Permanent address: Central Laboratory of Photoprocesses, Bulgarian Academy of Sciences, 1040 Sofia, Bulgaria.

[1] W. Krätschmer, L.D. Lamb, K. Fostiropoulos, and D.R. Huffman, Nature (London) **347**, 354 (1990).
[2] P.A. Heiney, J.E. Fischer, A.R. McGhie, W.J. Romanow, A.M. Denenstein, J.P. McCauley, Jr., A.B. Smith III, and D.E. Cox, Phys. Rev. Lett. **66**, 2911 (1991).
[3] A. Cheng, M.L. Klein, and C. Caccamo, Phys. Rev. Lett. **71**, 1200 (1993).
[4] C. Caccamo, D. Costa, and A. Fucile, J. Chem. Phys. **106**, 255 (1997).
[5] M. Hasegawa and K. Ohno, J. Chem. Phys. **111**, 5955 (1999).
[6] A.L.C. Ferreira, J.M. Pacheco, and J.P. Prates-Ramalho, J. Chem. Phys. **113**, 738 (2000).
[7] M.H.J. Hagen, E.J. Meijer, G.C.A.M. Mooij, D. Frenkel, and H.N.W. Lekkerkerker, Nature (London) **365**, 425 (1993).
[8] J.Q. Broughton, J.V. Lill, and J.K. Johnson, Phys. Rev. B **55**, 2808 (1997).
[9] T.P. Martin, U. Näher, H. Schaber, and U. Zimmermann, Phys. Rev. Lett. **70**, 3079 (1993).
[10] A.L. Mackay, Acta Crystallogr. **15**, 916 (1962).
[11] K. Hansen, H. Hohmann, R. Müller, and E.E.B. Campbell, J. Chem. Phys. **105**, 6088 (1996).
[12] K. Hansen, R. Müller, H. Hohmann, and E.E.B. Campbell, Z. Phys. D: At., Mol. Clusters **40**, 361 (1997).
[13] L.A. Girifalco, J. Phys. Chem. **96**, 858 (1992).
[14] J.M. Pacheco and J.P. Prates-Ramalho, Phys. Rev. Lett. **79**, 3873 (1997).
[15] K.-P. Bohnen and R. Heid, Phys. Rev. Lett. **83**, 1167 (1999).
[16] M. Sprik, A. Cheng, and M.L. Klein, J. Phys. Chem. **96**, 2027 (1992).
[17] Z. Gamba, Phys. Rev. B **57**, 1402 (1998).
[18] J.P. Lu, X.-P. Li, and R.M. Martin, Phys. Rev. Lett. **68**, 1551 (1992).
[19] C. Rey and L.J. Gallego, Phys. Rev. E **53**, 2480 (1996).
[20] H. Guérin, J. Phys. Condens. Matter **10**, L527 (1998).
[21] C. Girard, P. Lambin, A. Dereux, and A.A. Lucas, Phys. Rev. B **49**, 11 425 (1994).
[22] J.P.K. Doye and D.J. Wales, Chem. Phys. Lett. **262**, 167 (1996).
[23] C. Rey, J. Garcia-Rodeja, and L.J. Gallego, Z. Phys. D: At., Mol. Clusters **40**, 395 (1997).
[24] For updated energy values, refer to the Cambridge Cluster Database (URL: http://brian.ch.cam.ac.uk/CCD.html), D. J. Wales, J. P. K. Doye, A. Dullweber, and F. Y. Naumkin.
[25] J.P.K. Doye, A. Dullweber, and D.J. Wales, Chem. Phys. Lett. **269**, 408 (1997).
[26] J. Garcia-Rodeja, C. Rey, and L.J. Gallego, Phys. Rev. B **56**, 6466 (1997).
[27] W. Zhang, L. Liu, J. Zhuang, and Y. Li, Phys. Rev. B **62**, 8276 (2000).
[28] J.P.K. Doye, D.J. Wales, W. Branz, and F. Calvo, Phys. Rev. B **64**, 235409 (2001).
[29] J.P.K. Doye, D.J. Wales, and R.S. Berry, J. Chem. Phys. **103**, 4234 (1995).
[30] J.P.K. Doye and D.J. Wales, J. Chem. Soc., Faraday Trans. **93**, 4233 (1997).
[31] R. Antoine, P. Dugourd, D. Rayane, E. Benichou, and M. Broyer, J. Chem. Phys. **110**, 9771 (1999).
[32] W. Branz, N. Malinowski, H. Schaber, and T.P. Martin, Chem. Phys. Lett. **328**, 245 (2000).
[33] R.H. Leary and J.P.K. Doye, Phys. Rev. E **60**, 6320 (1999).
[34] J.P.K. Doye and D.J. Wales, Phys. Rev. Lett. **80**, 1357 (1998).
[35] C.L. Cleveland, W.D. Luedtke, and U. Landman, Phys. Rev. Lett. **81**, 2036 (1998).
[36] C.L. Cleveland, W.D. Luedtke, and U. Landman, Phys. Rev. B **60**, 5065 (1999).
[37] J.P. Neirotti, F. Calvo, D.L. Freeman, and J.D. Doll, J. Chem. Phys. **112**, 10340 (2000).
[38] F. Calvo, J.P.K. Doye, and D.J. Wales, Phys. Rev. Lett. **87**, 119301 (2001).
[39] J.P.K. Doye and F. Calvo, Phys. Rev. Lett. **86**, 3570 (2001).
[40] F. Baletto, C. Mottet, and R. Ferrando, Phys. Rev. Lett. **84**, 5544 (2000).
[41] F. Baletto, J.P.K. Doye, and R. Ferrando, Phys. Rev. Lett. **88**, 075503 (2002).
[42] W. Branz, Ph.D. thesis, University of Stuttgart, 2001.
[43] T.P. Martin, U. Näher, H. Schaber, and U. Zimmermann, J. Chem. Phys. **100**, 2322 (1994).
[44] The duration of stay of the clusters in the heating cell (stability region) was determined by alternately ionizing them with focused laser pulses at the entrance and the exit of the heating cell. Afterwards the time was measured that the created ion packet needed to reach the ionization volume of the TOF spectrometer.
[45] M. Schmidt, R. Kusche, W. Kronmüller, B.v. Issendorff, and H. Haberland, Phys. Rev. Lett. **79**, 99 (1997).
[46] For a detailed description of the method see, for example, W. Forst, *Theory of Unimolecular Reactions* (Academic Press, New York, 1973).
[47] M.S. Baba, T.S.L. Narasimhan, R. Balasubramanian, N. Sivaraman, and C.K. Mathews, J. Phys. Chem. **98**, 1333 (1994).
[48] C.K. Mathews, M.S. Baba, T.S.L. Narasimhan, R. Balasubramanian, N. Sivaraman, T.G. Srinivasan, and P.R.V. Rao, J. Phys. Chem. **96**, 3566 (1992).
[49] C.K. Mathews, M.S. Baba, T.S.L. Narasimhan, R. Balasubramanian, N. Sivaraman, T.G. Srinivasan, and P.R.V. Rao, Fullerene Sci. Technol. **1**, 101 (1993).
[50] C. Pan, M.P. Sampson, Y. Chai, R.H. Hauge, and J.L. Margrave, J. Phys. Chem. **95**, 2944 (1991).
[51] J. Abrefah, D.R. Olander, M. Balooch, and W.J. Siekhaus, Appl. Phys. Lett. **60**, 1313 (1992).
[52] M. Moalem, M. Balooch, A.V. Hamza, and R.S. Ruoff, J. Phys. Chem. **99**, 16736 (1995).
[53] Note that $\alpha_{SI}=4\pi\varepsilon_0\alpha_{cgs}$.
[54] O. Echt, K. Sattler, and E. Recknagel, Phys. Rev. Lett. **47**, 1121 (1981).
[55] I.A. Harris, R.S. Kidwell, and J.A. Northby, Phys. Rev. Lett. **53**, 2390 (1984).
[56] J. Farges, M.F. de Feraudy, B. Raoult, and G. Torchet, J. Chem. Phys. **84**, 3491 (1986).
[57] J.A. Northby, J. Chem. Phys. **87**, 6166 (1987).
[58] J.P.K. Doye, M.A. Miller, and D.J. Wales, J. Chem. Phys. **111**, 8417 (1999).
[59] L.D. Marks, Philos. Mag. A **49**, 81 (1984).

[60] D. Tomanek (private communication).
[61] J.P.K. Doye, M.A. Miller, and D.J. Wales, J. Chem. Phys. **110**, 6896 (1999).
[62] D.J. Wales, M.A. Miller, and T.R. Walsh, Nature (London) **394**, 758 (1998).
[63] J.P.K. Doye, D.J. Wales, and M.A. Miller, J. Chem. Phys. **109**, 8143 (1998).
[64] M.A. Miller, J.P.K. Doye, and D.J. Wales, J. Chem. Phys. **110**, 328 (1999).
[65] D.J. Wales, J. Chem. Phys. **101**, 3750 (1994).
[66] M.A. Miller, J.P.K. Doye, and D.J. Wales, Phys. Rev. E **60**, 3701 (1999).
[67] P.M. Morse, Phys. Rev. **34**, 57 (1929).
[68] M.S. Deleuze and F. Zerbetto, J. Am. Chem. Soc. **121**, 5281 (1999).
[69] H.C. Andersen, J. Chem. Phys. **72**, 2384 (1980).
[70] In order to make reliable conclusions we performed five to ten independent MD runs at each temperature.